

A New Constitutive Model for the High-Temperature Flow Behavior of 95CrMo Steel

Bao-Sheng Xie, Qing-Wu Cai, Yu Wei, Li-Xiong Xu, and Ning Zhen

(Submitted April 18, 2016; in revised form September 28, 2016; published online October 13, 2016)

The compressive deformation behavior of 95CrMo steel, one of the worldwide used hollow steels, was investigated on a Gleeble-3500 thermo-simulation machine within temperature range of 1073–1323 K and strain rate range of 0.1–10 s⁻¹. Considering the influence of work-hardening, dynamic recovery and dynamic recrystallization, a new constitutive model for high-temperature flow stress was established in this paper. The calculated values predicted by the new constitutive model lie fairly close to the experimental values with a correlation coefficient (*R*) of generally above 0.99 and an average absolute relative error of 3.00%, proving a good predictability of the new constitutive model. Also, a modified Sellars-Tegart-Garofalo model (STG model) was introduced to verify the precision of the new constitutive model. Compared to the modified STG model, the new constitutive model has a higher accuracy, which implies it is a reliable tool for predicting flow stress at high temperatures not only under equilibrium state, but also under transient deformation conditions. Besides, the new constitutive model was proved still viable in the initial stage of plastic deformation where plastic strain is lower than 0.05.

Keywords 95CrMo, constitutive model, flow stress, hot compression

1. Introduction

With the development of numerical simulation, finite element (FE) method has been successfully employed to analyze and optimize forming technique of materials, such as forging, rolling and extrusion (Ref 1). During the development of FE simulation model, constitutive equation for flow stress is a crucial parameter to improve the applicability and reliability of numerical simulation. Therefore, an accurate constitutive equation is essential to simulate and optimize the forming process (Ref 2).

A constitutive model for flow behavior at high temperature generally contains two parts. Firstly, a reasonable model should be required to describe the characteristic stresses (yield stress, peak stress and saturation stress, for instance) which are the stresses under equilibrium state and determined by work-hardening (WH), dynamic recovery (DR) and recrystallization (DRV). Secondly, proper equations would be identified to describe transient stress in the whole strain range, and the transient stress depends on the combined effects of WH, DR and DRV. According to previous references (Ref 3–5), common models for characteristic stress are composed of power-law equation (Eq 1), exponential equation (Eq 2) and hyperbolic-

sine equation (Eq 3). As claimed by many researches, hyperbolic-sine equation, which was usually referred as the Sellars-Tegart-Garofalo (STG) model, can predict flow stress over a wide range of strain rate and temperatures as it combines both power-law and exponential dependences in the low and high stress limits, respectively. Besides, taking the influence of deformation temperature on shear modulus and athermal stress into account, physically based phenomenological models were established (Ref 6). More recently, Galindo-Nava and Rivera-Díaz-del-Castillo (Ref 7) proposed a novel thermo-statistical approach to describe hot deformation of unary and multicomponent FCC alloys.

As for transient stress within the whole strain range, vast majority of the common strain-stress equations proposed for the description of the high-temperature flow stress include the equations deriving from Estrin-Mecking equation, the hyperbolic-sine equations (hereafter referred to as ‘modified STG model’) considering the parameters (*A*, *Q*, *α*, *n* in Eq 3) of the STG model as functions of strain, and the work-hardening law (hereafter referred to as ‘Sah based model’) proposed by Sah et al. (Ref 8). As to Estrin-Mecking equation that describes the development of dislocation density during high-temperature deformation, Lin et al. (Ref 9) investigated the compressive deformation behavior of 42CrMo steel and proposed a constitutive model. In case of the modified STG model, Sloof et al. (Ref 10) considered the influence of strain on the apparent material constants and proposed modified strain-dependent equations to predict the high-temperature flow stress; whereafter, Lin et al. (Ref 11) claimed the strain-dependent equations were not sufficient for accurately predicting flow behavior, and put forward a modified STG model by compensating the strain rate in the Zener-Hollomon parameter. Recently, Xu et al. (Ref 12) tried to optimize some parameters and obtained a more accurate model. In terms of the work-hardening law, Puchi-Carera et al. (Ref 13) updated the changes in deformation temperature and strain rate, and integrated work-hardening law to compute flow stress from the previous value.

Bao-Sheng Xie, **Li-Xiong Xu**, and **Ning Zhen**, Collaborative Innovation Center of Steel Technology of USTB, Beijing 100083, China; **Qing-Wu Cai**, Collaborative Innovation Center of Steel Technology of USTB, Beijing 100083, China; and National Engineering Research Center of Advanced Rolling of USTB, Beijing 100083, China; **Yu Wei**, National Engineering Research Center of Advanced Rolling of USTB, Beijing 100083, China. Contact e-mails: xiebaoshenghql@gmail.com and caiqw@nercar.ustb.edu.cn.

$$\dot{\epsilon} = B_1 \sigma^\beta \quad (\text{Eq 1})$$

$$\dot{\epsilon} = B_2 \exp(\gamma \sigma) \quad (\text{Eq 2})$$

$$Z = \dot{\epsilon} \exp\left(\frac{Q}{RT}\right) = A[\sinh(\alpha \sigma)]^n \quad (\text{Eq 3})$$

where A , B_1 , B_2 , α , β , γ are material constants, n the stress exponent, Q the activation energy, T the temperature, $\dot{\epsilon}$ the strain rate and R the gas constant (8.314 J/mol/K).

As one of the worldwide used hollow steels, 95CrMo steels are characterized by excellent strength, high wear resistance and good hardening capacity as well as fine fatigue resistance. After rolling or normalizing at 850-870 °C, the 95CrMo steels consisted by the microstructures of troostite and sorbite can exhibit excellent mechanical properties and hardness. Hence, a concise rolling process of 95CrMo steels could be feasible, and hot deformation behavior of 95CrMo steels plays a more significant role on microstructures and performance (Ref 14). Even so, 95CrMo steels were seldom involved in existent researches and always referred to GCr15 steels (Ref 15-17). To the authors' knowledge, the constitutive equation of 95CrMo steel under hot deformation condition is still unavailable.

The aim of this study is to investigate the effects of strain rate and temperature on hot working behavior, and to formulate the thermo-plastic constitutive equation for establishing the FE model of 95CrMo steel. For this, the experimental hot compression tests were conducted within temperature range of 1073-1323 K and strain rate range of 0.1-10 s⁻¹. In this paper, a new strain-stress relationship during entire plastic deformation was proposed, and the characteristic stresses were computed by hyperbolic-sine equation, and the validity of the developed constitutive equations was also confirmed by statistics estimators. Moreover, to further study the precision of the constitutive model proposed in the present paper, the relatively new modified STG model was introduced, and the comparison of the two models was made to verify the model developed in this paper.

2. Experiments

Chemical composition of the 95CrMo hypereutectoid steel used in the present study is 0.95C-0.22Si-0.25Mn-1.21Cr-0.28Mo-0.02Cu-0.01V-(bal.)Fe, and the initial microstructures are showed in Fig. 1. The specimens were cut by spark wire cutting from 95CrMo steel rolled by Guiyang Special Steel, and the detailed process of the as-received 95CrMo steel was presented in Ref 18. The cylindrical specimens (diameter: 10 mm, length: 15 mm) for compression tests were machined by spark wire cutting. Hot compression tests were conducted using a Gleeble 3500 thermal simulation machine. Specimens were firstly heated to 1373 K at a rate of 20 K/s, and soaked for 2 min to completely dissolve the precipitates, and subsequently cooled to deformation temperature at a rate of 10 K/s. The specimens were then held isothermally for 20 s before compression to maintain a uniform temperature distribution throughout the cylinders. The reduction in height is 60% at the end of compression tests, and the specimens were cooled to room temperature in the atmosphere of argon subsequently after compression (the average cooling rates in the atmosphere of argon were 10.3 K/s measured from time-temperature curves).

The compression temperatures were ranging from 1073 to 1323 K at intervals of 50 K, and constant true strain rates were set as 0.1, 1, 3 and 10 s⁻¹. The true stress-true strain data were recorded automatically during isothermal compression.

3. Results and Discussion

3.1 True Stress-Strain Curves

Due to the combined effects of work-hardening and thermally activated softening mechanisms (Ref 2), most of the flow stress curves can be classified into three types: work-hardening, characterized by increasing stress with the increasing strain; dynamic recovery, characterized by saturation stress (σ_{DR}) with the increasing strain; dynamic recrystallization, characterized by an observed peak stress prior to steady stress (σ_{SS}).

The true stress-strain curves obtained from hot compression of 95CrMo steel are represented in Fig. 2. It can be seen, with the increase in temperature or decrease in strain rate, the flow stress decreases. When strain rate is 0.1 s⁻¹ and deformation temperature is more than 1173 K, the flow stress curves exhibit typical dynamic recrystallization behavior with a single-peak stress followed by a gradual fall toward a steady stress (σ_{SS}). However, the other curves exhibit work-hardening stage and dynamic recovery stage.

From stress-strain curves in Fig. 2, the characteristic stresses (yield strength, peak stress as well as saturation stress) were obtained. In some studies, yield strength was set to a fixed value in different conditions, such as 14.74 MPa in Ref 2; besides, the true plastic strain is almost replaced by true strain (Ref 12, 24). In order to describe the flow stress more accurately, the flow stress data were firstly fitted by polynomial regression according to Song et al. (Ref 19); then with the help of MATLAB software and the method of stepwise mathematics in GB/T 228-2002, the yield stress can be calculated; finally based on Samantaray et al. (Ref 20), the true stress-true plastic strain curves were obtained by subtracting the elastic region from the true stress-true strain curves.

3.2 Characteristic Stress

In researches regarding hot working, the Arrhenius equation is widely used to describe the relationship between strain rate, flow stress and temperature, especially at high temperature. The hyperbolic law in an Arrhenius-type equation as shown in Eq 3 represents a more accurate relationship between the Zener-Hollomon parameter (Z) and stress (Ref 21). It should be noted that σ in Eq 2 is the steady-state stress due to dynamic recovery, σ_{DR} . Based on Eq 3, flow stress can be written as a function of Z as shown in Eq 4.

$$\sigma = \frac{1}{\alpha} \ln \left\{ \left(\frac{Z}{A} \right)^{1/n} + \left[\left(\frac{Z}{A} \right)^{2/n} + 1 \right]^{1/2} \right\} \quad (\text{Eq 4})$$

The power type Eq 1 and exponential Eq 2 are suitable for low stress level ($\alpha \sigma < 0.8$) and high stress level ($\alpha \sigma > 1.2$), respectively (Ref 11). Hence, under the deformation strain of 0.05, the material constants (γ , β) can be obtained, and then, α can be calculated as γ/β . The logarithm of Eq 1-2 yields the following Eq 5a-5b. By substituting the flow stress under the strain of 0.05 and corresponding strain rate into Eq 5a-5b, the

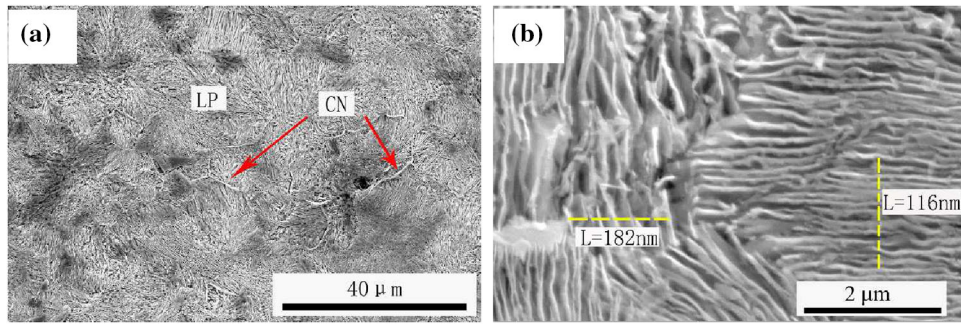


Fig. 1 Microstructure of as-received drilling steel (a) overall microstructure at lower magnification (b) detailed microstructure of pearlite. LP—lamellar pearlite; CN—cementite network; L—average pearlite lamellar spacing

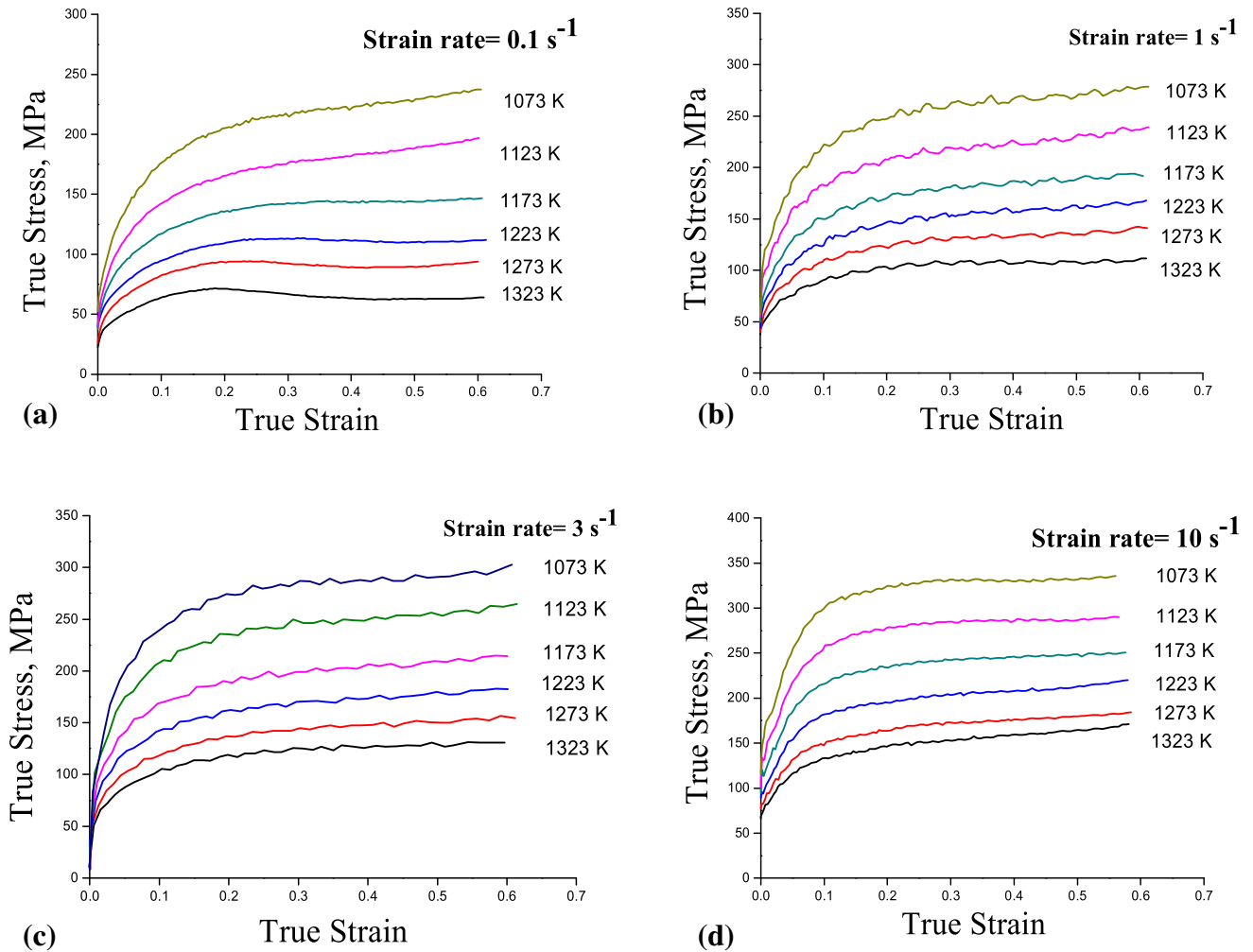


Fig. 2 True stress-strain curves for 95CrMo steel under the different deformation temperatures and strain rates. (a) 0.1 s^{-1} (b) 1 s^{-1} (c) 3 s^{-1} (d) 10 s^{-1}

mean γ and β were obtained as 8.066 and 0.0746 MPa^{-1} , respectively. Hence, $\alpha = \gamma/\beta = 0.009547 \text{ MPa}^{-1}$, which was similar to the value of Ref 11 ($\alpha = 0.0093 \text{ MPa}^{-1}$) and Ref 22 ($\alpha = 0.01125 \text{ MPa}^{-1}$). It is noteworthy that α is generally a fixed value for each family of alloys related to the characteristic stress range, and was reported as 0.014 MPa^{-1} for carbon steels and HSLA steels, but the addition of alloy element, such as Cr, Mo, Cu, Ni, has important effects on α and makes $\alpha = 0.012 \text{ MPa}^{-1}$ (Ref 4) in stainless steels which contain

relatively high contents of Ni, Cr, Cu. Therefore, the relatively lower value of α in this paper might result from the addition of alloy elements.

$$\ln \sigma = \frac{1}{\beta} \ln \dot{\epsilon} - \frac{1}{\beta} \ln B_1 \quad (\text{Eq 5a})$$

$$\sigma = \frac{1}{\gamma} \ln \dot{\epsilon} - \frac{1}{\gamma} \ln B_2 \quad (\text{Eq 5b})$$

where B_1, B_2, β, γ are material constants, and $\alpha = \gamma/\beta$.

By differentiating Eq 3, the value of n can be written as Eq 6a. Hence, substituting the flow stress and strain rate at all temperatures into Eq 6a, the value of n can be obtained as 4.676 from the slope of the line in the $\ln(\text{Ref} \sinh(\alpha\sigma))$ vs. $\ln \dot{\epsilon}$ plot (shown in Fig. 3a). By differentiating Eq 3, the value of Q can be expressed as Eq 6b. Substituting the flow stress and temperature for all strain rates, the value of Q can be derived from the slope of the line in the $Rn \ln(\text{Ref} \sinh(\alpha\sigma))$ versus $1/T$ plot (shown in Fig. 3b). The deformation activation energy, Q , was obtained as 336.41 ± 12.28 kJ/mol by averaging the values of Q at different strain rates. Then, through the intercept of $\ln(\text{Ref} \sinh(\alpha\sigma))$ versus $\ln \dot{\epsilon}$ plot, the parameter, $\ln A$, can be easily obtained as 29.420 ± 0.224 by averaging the values of $\ln A$ at different temperatures.

$$n = \frac{\partial \ln \dot{\epsilon}}{\partial \ln [\sinh(\alpha\sigma)]} \quad (\text{Eq 6a})$$

$$Q = Rn \frac{\partial \ln [\sinh(\alpha\sigma)]}{\partial (1/T)} \quad (\text{Eq 6b})$$

According to the above analysis and methods, the equation for steady stress due to DR and WH of as well as for saturation stress due to WH, DR and DRV can be derived as Eq 7. Comparison of experimental and calculated stress is showed in Fig. 4, in which the calculated stresses were fairly close to the experimental stresses and a satisfactory prediction of the equations was indicated by high correlation coefficient (R).

$$\begin{cases} \sigma_{\text{DR}} = 105.74 \ln \left\{ \left(\frac{Z}{5.9823 \times 10^{12}} \right)^{1/4.676} + \left[\left(\frac{Z}{5.9823 \times 10^{12}} \right)^{2/4.676} + 1 \right]^{1/2} \right\} \\ \sigma_{\text{SS}} = 105.74 \ln \left\{ \left(\frac{Z}{9.4749 \times 10^{12}} \right)^{1/4.676} + \left[\left(\frac{Z}{9.4749 \times 10^{12}} \right)^{2/4.676} + 1 \right]^{1/2} \right\} \end{cases} \quad (\text{Eq 7})$$

3.3 Constitutive Equations

Considering the influence of dynamic recovery, flow stress at high temperature is determined by the balance of WH due to dislocation multiplication and DR resulting from dislocation annihilation in metals (Ref 23, 24). In present work, an appropriate work-hardening law for transient stress affected by WH and DR has been achieved by the exponential saturation work-hardening law proposed by Sah et al. as expressed by Eq 8a. In Eq 8a, $\sigma_y(T, \dot{\epsilon})$ represents the yield strength under deformation temperature (T) and strain rate ($\dot{\epsilon}$), $\sigma_{\text{DR}}(T, \dot{\epsilon})$ is the steady stress due to DR and WH, $\mu(T)$ is shear modulus determined by temperature and could be calculated by Eq 8b, θ is material constant that could be calculated from the measured flow stress curves, μ_0 represents the shear modulus at 0 K and equals to 88884.6 MPa, T is the absolute temperature, and ϵ is virtually true plastic strain. Puchi-Cabrera et al. (Ref 13) also used this law to develop a rational description of work-hardening rate for a C-Mn steel. In their studies, the temperature and strain rate dependences of the yield saturation stress

were implemented at first, and then, the changes that might occur in plastic deformation were updated in each strain interval, and then, the numerical integration of Eq 8a was employed to compute the flow stress from its previous value.

$$\frac{\partial \sigma}{\partial \epsilon} = \frac{\mu(T)}{\theta} \left[1 - \left(\frac{\sigma - \sigma_y(T, \dot{\epsilon})}{\sigma_{\text{DR}}(T, \dot{\epsilon}) - \sigma_y(T, \dot{\epsilon})} \right)^2 \right] \left[\frac{\sigma_{\text{DR}}(T, \dot{\epsilon}) - \sigma_y(T, \dot{\epsilon})}{\sigma - \sigma_y(T, \dot{\epsilon})} \right] \quad (\text{Eq 8a})$$

$$\mu(T) = \mu_0 - 37.3T \quad (\text{Eq 8b})$$

Despite this, the parametric solution and procedures including numerical integration, recursion and updating in their model were rather complicated. So, it is gratifying that integration and recursion can be eliminated but the high precision could be kept. In order to achieve this, in this paper, we firstly assumed θ in Eq 8a is a variable depending on strain rate and temperature; therefore, Eq 8a turns into a differential equation of strain and stress. Secondly, the differential equation was solved, and the relationship between stress and strain can be obtained and represented by Eq 9a. From Eq 9a, transient stress affected by WH and DR was determined by σ_{DR} , yield stress, plastic strain and a material constant θ . Apparently, θ is the slope in the lines of $\frac{(\sigma_{\text{DR}}(T, \dot{\epsilon}) - \sigma_y(T, \dot{\epsilon}))}{2\mu(T)} \ln \left(1 - \left(\frac{\sigma - \sigma_y(T, \dot{\epsilon})}{\sigma_{\text{DR}}(T, \dot{\epsilon}) - \sigma_y(T, \dot{\epsilon})} \right)^2 \right)$ versus true plastic strain plots (as represented in Eq 9b). In this paper, in order to eliminate the influence of DRV and reduce the errors in regressions, the true plastic strain in the range of 0-0.20 and the corresponding stress were utilized to calculate θ . The procedures to determine θ under different deformation conditions are

showed in Fig. 5, and the measured values are represented in Fig. 6. With the formula conversions of Eq 9a, 9c could be obtained. So, if the right parts of Eq 9c and the evolution equation (as shown in Eq 10) deriving from Estrin-Mecking equation are considered as plausible kinetics for dynamic recovery, the two equations are exactly similar.

The Arrhenius equation is always used to describe the relationship between strain rate, flow stress and temperature, particularly for deformations at high temperature. The following typical equation containing the Arrhenius equation (Eq 11a) was employed to describe the effects of $\dot{\epsilon}$ and T of on θ , just as it was applied to dynamic recovery coefficient, Ω , in Eq 10 (Ref 2, 9). In Eq 11a, φ and m_θ are constants, R is the universal gas constant (8.314 J/mol/K), and Q_θ is activation energy.

$$\sigma = \sigma_y(T, \dot{\epsilon}) + [\sigma_{\text{DR}}(T, \dot{\epsilon}) - \sigma_y(T, \dot{\epsilon})] \sqrt{1 - \exp \left[-\frac{2\mu(T)\epsilon}{\theta \{ \sigma_{\text{DR}}(T, \dot{\epsilon}) - \sigma_y(T, \dot{\epsilon}) \}} \right]} \quad (\text{Eq 9a})$$

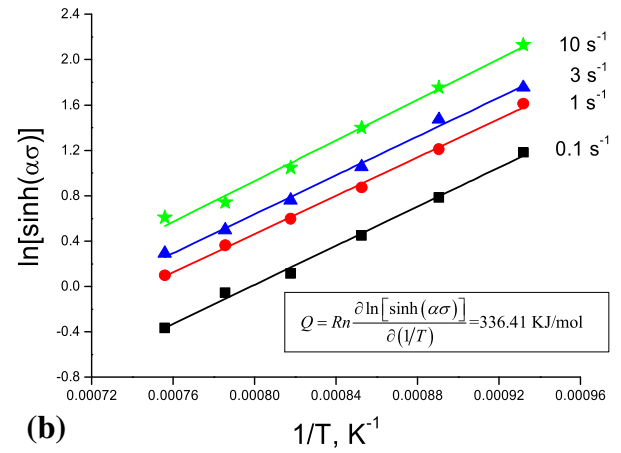
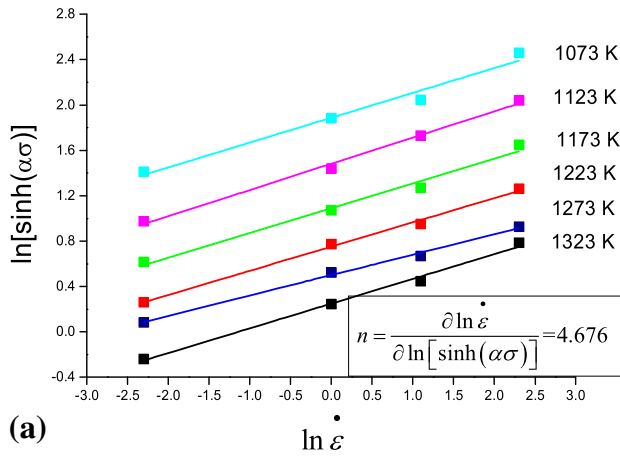


Fig. 3 Determinations of the coefficients n (a) and Q (b) in Eq 3 at different deformation temperatures

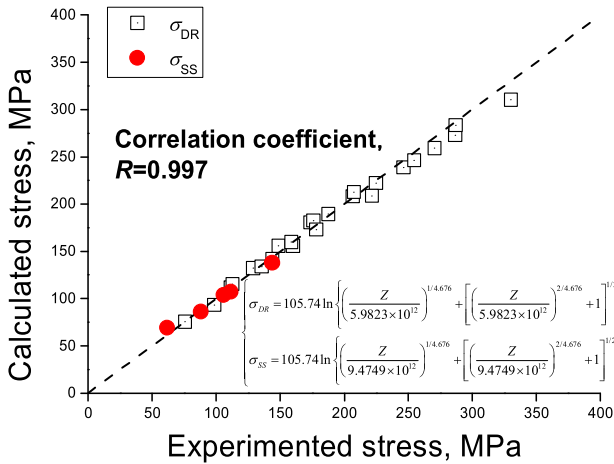


Fig. 4 Comparisons between the experimented and calculated characteristic stresses

$$\frac{(\sigma_{DR}(T, \dot{\epsilon}) - \sigma_y(T, \dot{\epsilon}))}{2\mu(T)} \ln \left(1 - \left(\frac{\sigma - \sigma_y(T, \dot{\epsilon})}{\sigma_{DR}(T, \dot{\epsilon}) - \sigma_y(T, \dot{\epsilon})} \right)^2 \right) = -\frac{\epsilon}{\theta} \quad (\text{Eq 9b})$$

$$1 - \left(\frac{\sigma - \sigma_y(T, \dot{\epsilon})}{\sigma_{DR}(T, \dot{\epsilon}) - \sigma_y(T, \dot{\epsilon})} \right)^2 = \exp \left[-\frac{2\mu(T)}{\theta(\sigma_{DR}(T, \dot{\epsilon}) - \sigma_y(T, \dot{\epsilon}))} \epsilon \right] \quad (\text{Eq 9c})$$

$$1 - \frac{\sigma^2(T, \dot{\epsilon}) - \sigma_y^2(T, \dot{\epsilon})}{\sigma_{DR}^2(T, \dot{\epsilon}) - \sigma_y^2(T, \dot{\epsilon})} = \exp(-\epsilon) \quad (\text{Eq 10})$$

$$\theta = \varphi \dot{\epsilon}^{m_\theta} \exp \left(-\frac{Q_\theta}{RT} \right) \quad (\text{Eq 11a})$$

By differentiating Eq 11a, the value of m_θ , Q_θ can be written as Eq 11b and 11c, respectively. Taking the results of Fig. 6 into Eq 11b-11c, a linear regression as represented in Fig. 7 results in the average values of -0.0725 and 49.83 kJ/mol for m_θ , Q_θ , respectively. Substituting the known parameters m_θ and Q_θ to Eq 11a, the average value of φ was determined as 13370.538. It should be noted the value of m_θ is fairly close to the reported m_Ω of 52.3 kJ/mol (Ref 23) and 57.2 kJ/mol (Ref 2).

$$m_\theta = \frac{\partial \ln \theta}{\partial \ln \dot{\epsilon}} \quad (\text{Eq 11b})$$

$$Q_\theta = -R \frac{\partial \ln \theta}{\partial (1/T)} \quad (\text{Eq 11c})$$

Dynamic recrystallization is a significant factor of softening mechanisms. The flow stress during dynamic recrystallization (σ_{DRX}) is related to σ_{DR} , the volume fraction of dynamic recrystallization (X_{DRX}) and the steady-state stress (σ_{SS}) where recrystallization is complete and continuous, and can be written as follows (Ref 2):

$$\sigma_{DRX} = \sqrt{\sigma_r^2 - X_{DRX}(\sigma_r^2 - \sigma_{SS}^2)} \quad (\text{Eq 12})$$

In general, the recrystallization fraction, X_{DRX} , is used to fit an Avrami type sigmoidal curve according to previous literatures. The dynamic recrystallization model for hypereutectic steels with chromium and molybdenum was obtained as follows (Ref 25):

$$X_{DRX} = 1 - \exp \left[-2.67 \left(\frac{\epsilon - \epsilon_c}{\epsilon_{0.5}} \right)^{1.036} \right] \quad (\text{Eq 13a})$$

$$\epsilon_{0.5} = 0.0087 d_0^{0.0841} \dot{\epsilon}^{0.1733} \exp(35484/RT) \quad (\text{Eq 13b})$$

$$\epsilon_c = c \cdot \epsilon_p \quad (\text{Eq 13c})$$

$$\epsilon_p = 0.0338 d_0^{0.0342} \dot{\epsilon}^{0.1968} \exp(23550/RT) \quad (\text{Eq 13d})$$

where $\epsilon_{0.5}$ is the strain of 50% dynamic recrystallization, which can be expressed as a function of initial grain size d_0 , strain rate $\dot{\epsilon}$ and absolute temperature T ; ϵ_p is the strain at the peak stress; ϵ_c is the critical strain for the onset of DRX; c is a constant between 0.67 to 0.86 and is assumed to be 0.83 (Ref 26); d_0 is the initial grain size (μm) and equals to 12 μm for the investigated steel. The constitutive equation of dynamic recrystallization was obtained based on Eq 14:

$$\sigma_{DRX} = \begin{cases} \sigma_r & \epsilon \leq \epsilon_c \\ \sqrt{\sigma_r^2 - X_{DRX}(\sigma_r^2 - \sigma_{SS}^2)} & \epsilon > \epsilon_c \end{cases} \quad (\text{Eq 14})$$

Above all, flow stress can be predicted through Eq 7-14, and the comparison between the experimental and predicted flow

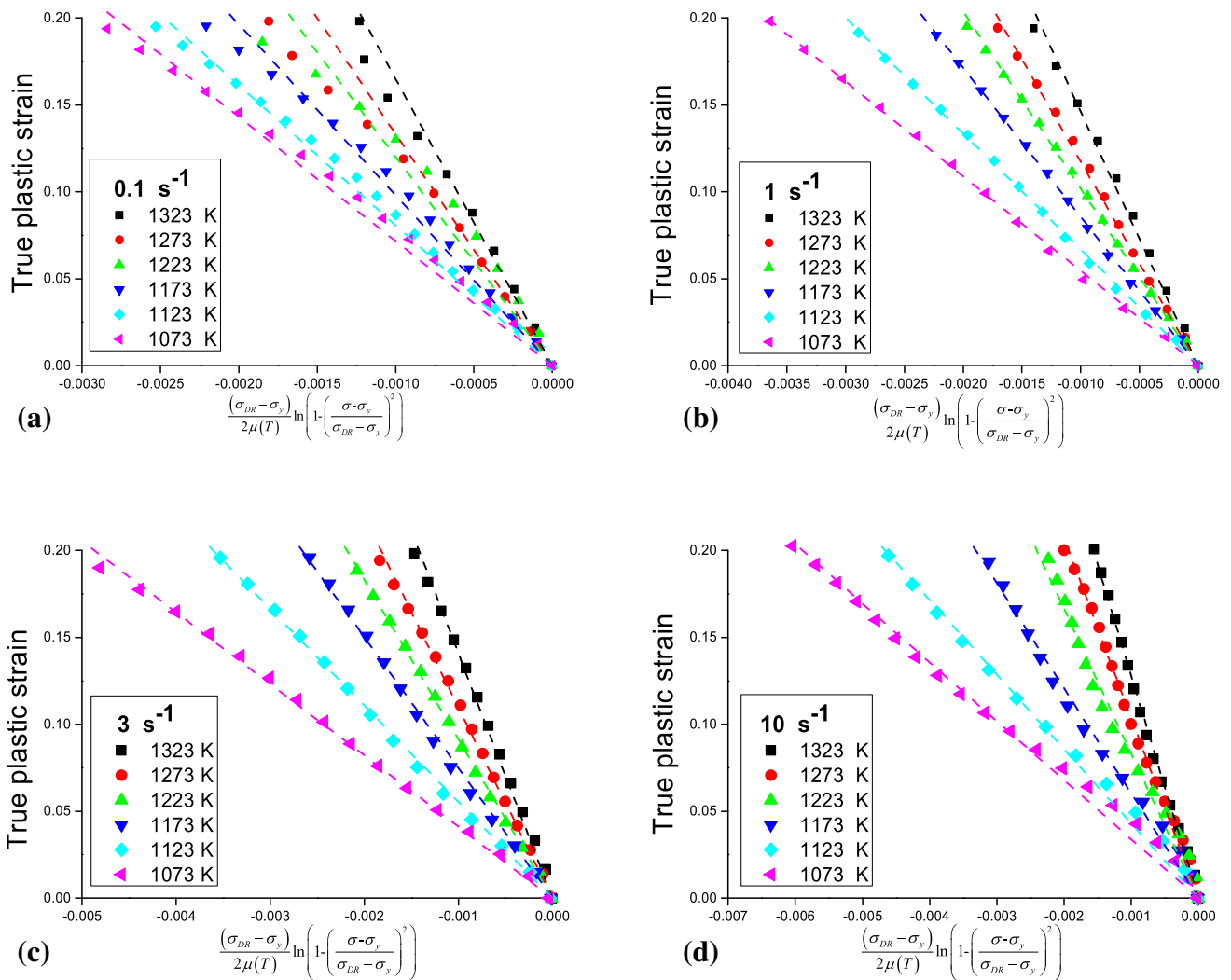


Fig. 5 Determinations of θ from the slope of $\frac{(\sigma_{DR}-\sigma_y)}{2\mu(T)} \ln\left(1-\left(\frac{\sigma-\sigma_y}{\sigma_{DR}-\sigma_y}\right)^2\right)$ vs. true plastic strain plot at different deformation. (a) 0.1 s^{-1} , (b) 1 s^{-1} , (c) 3 s^{-1} , (d) 10 s^{-1} . Note: σ_{DR} in the axis titles represents the abbreviation of $\sigma_{DR}(T, \dot{\epsilon})$ in present paper; σ_y in the axis titles shortens from $\sigma_y(T, \dot{\epsilon})$

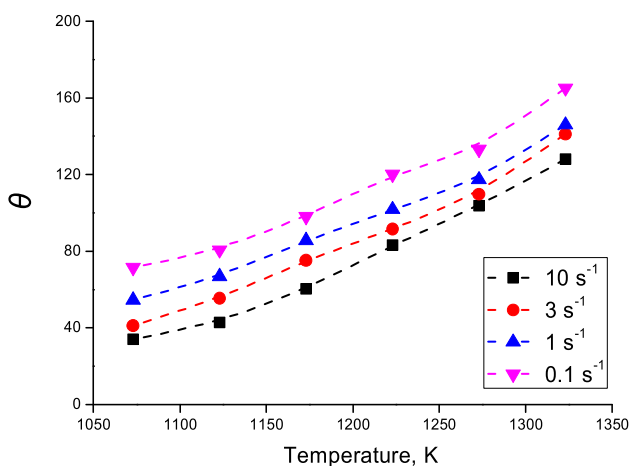


Fig. 6 Changes of θ with compression temperatures under different strain rate

stress is showed in Fig. 8 and 9. It can be seen that the predicted results are well matched with the experimental flow stresses. Here, it can be noticed that most of stress deviation was encompassed within a scatter band of $\pm 20 \text{ MPa}$, which indicates the high accuracy of the new constitutive model. Also, the high correlation coefficients, R , of more than 0.995 can verify a good prediction.

3.4 Verification of the Constitutive Equations

In order to have a further understanding of the accuracy of the new constitutive equations proposed in this study, the relatively new modified STG model was introduced. The introduced STG model considered the parameters (such as A , Q , α , n in Eq 3) as functions of strain according to Sloof et al. (Ref 10). Besides, the parameter optimizations of Xu et al. (Ref 12) were utilized to improve the accuracy of the modified STG model. According to Ref 12, β is the constant under the condition of high temperature and low strain rate, and should be chosen as the value of high temperature (1323 K for present paper); γ is under the condition of low

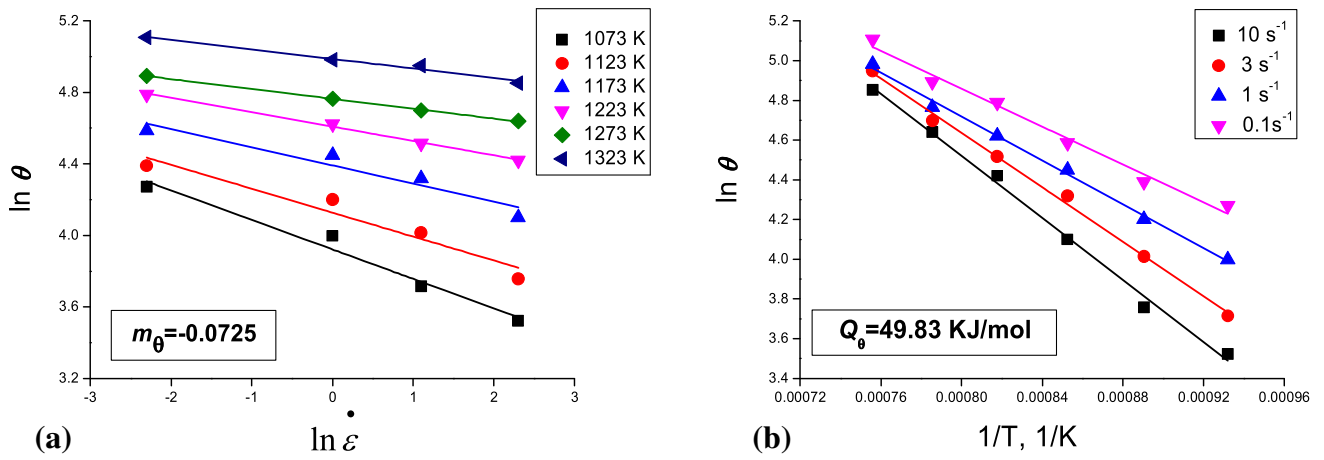


Fig. 7 Determinations of m_0 , Q_0 at different temperatures and strain rates. (a) m_0 , (b) Q_0

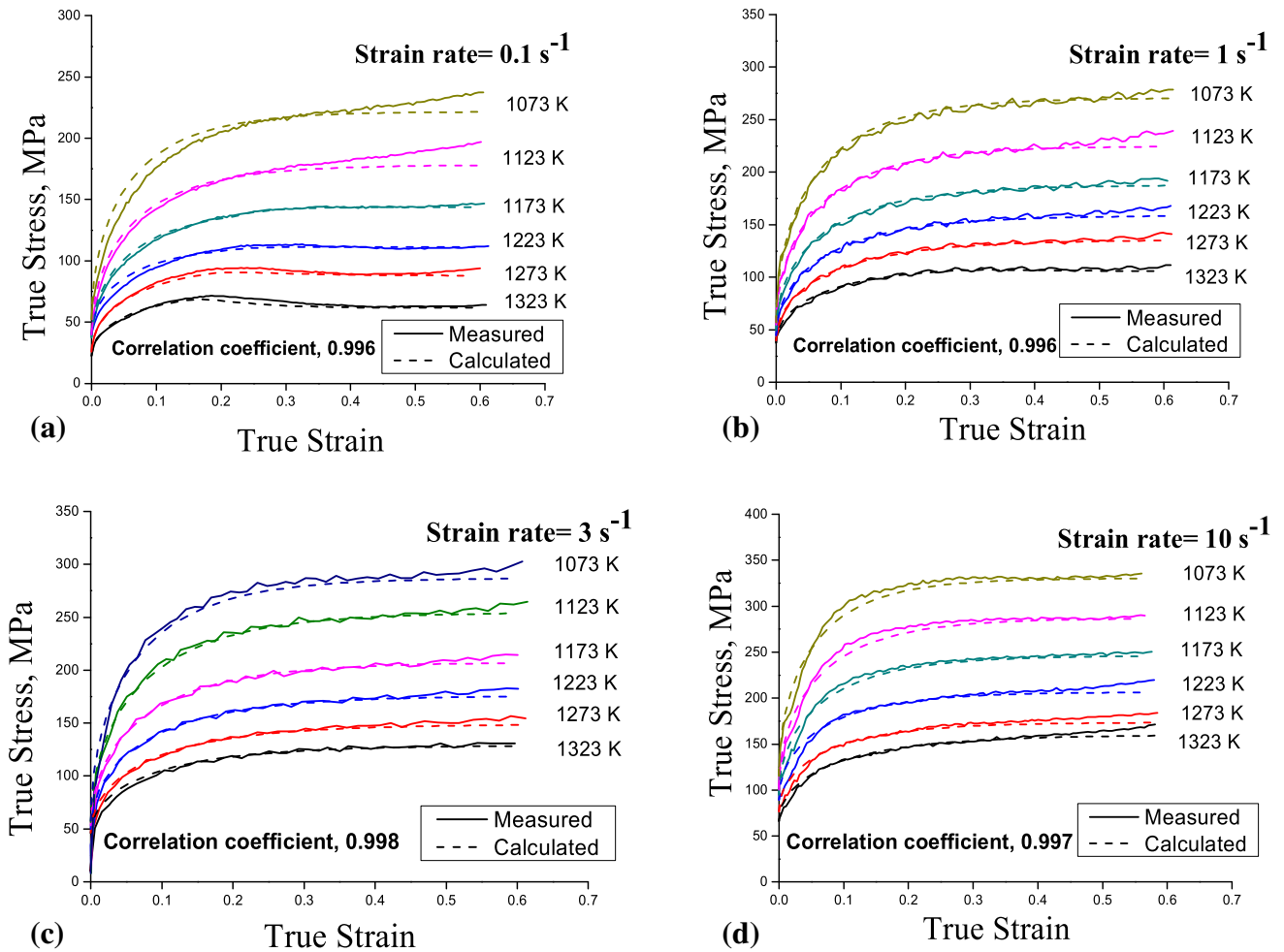


Fig. 8 Experimental and predicted flow stress of the new constitutive equations at different deformation conditions. (a) 0.1 s^{-1} , (b) 1 s^{-1} , (c) 3 s^{-1} , (d) 10 s^{-1}

temperature and high strain rate, and should be the value of low temperature (1073 K in this paper). Using the same solving process in section 3.2 and employing the strain within the range of 0.05-0.60 with an interval of 0.05 and

corresponding stress, the material constants (α , Q , $\ln A$, n) are computed and showed in Fig. 10. Fourth-order polynomial regressions as shown in Eq 15 led to the fitting results provided in Table 1.

Table 1 Polynomial fitting results of α , n , Q , and $\ln A$ of 95CrMo steel

i	C_{i0}	C_{i1}	C_{i2}	C_{i3}	C_{i4}
α	0.0102	-0.0759	0.401	-0.7449	0.4783
n	4.2605	31.521	-161.88	283.99	-169.86
Q	272.61	565.01	-853.40	-748.29	1727.07
$\ln A$	25.46	103.02	-409.47	604.79	-298.16

C_{ij} represents the j th-order coefficient of the dependent variable i

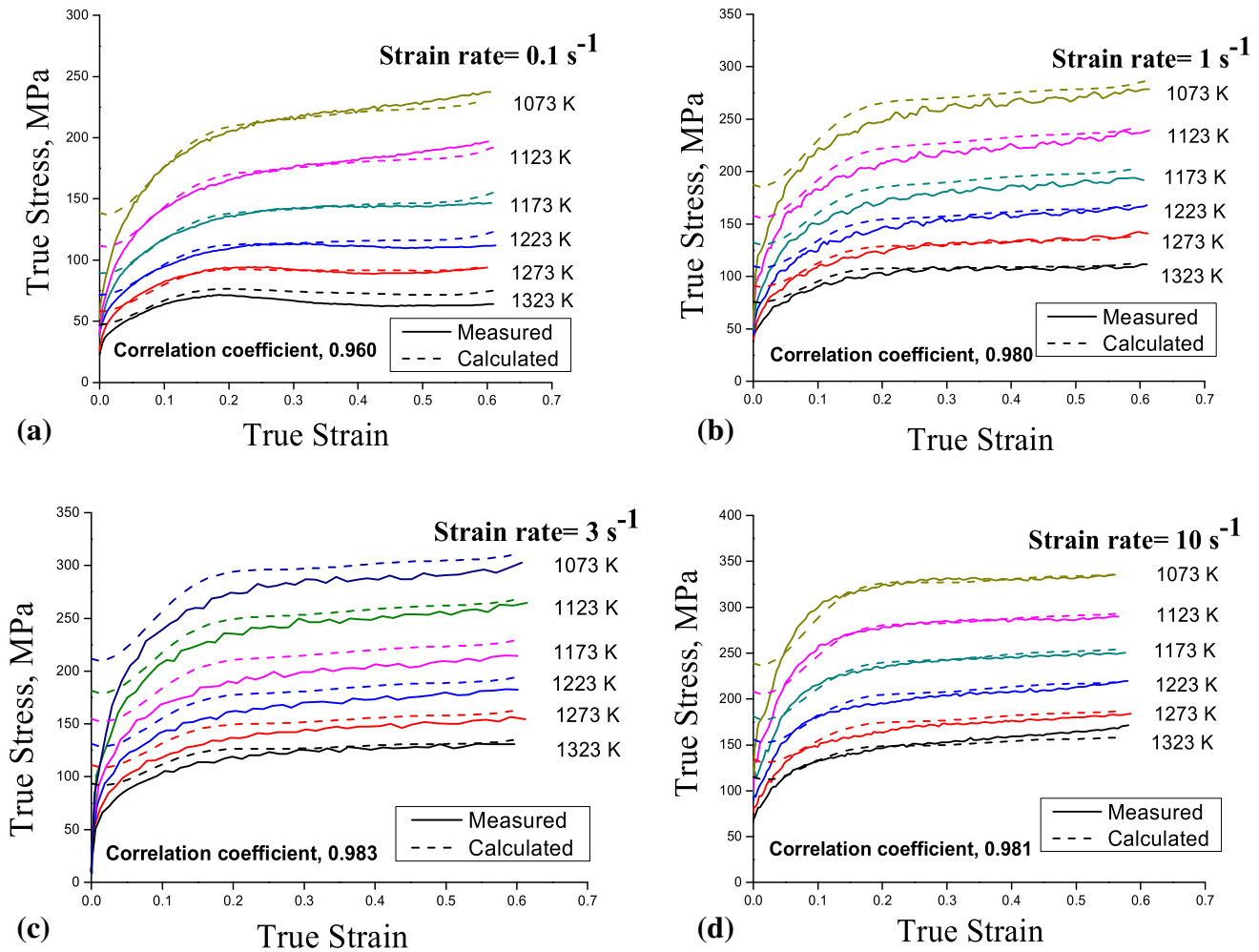


Fig. 11 Experimental and predicted flow stress of the modified STG model at hot deformation at different deformation conditions. (a) 0.1 s^{-1} , (b) 1 s^{-1} , (c) 3 s^{-1} , (d) 10 s^{-1}

and 29.66 when strain is 0.05. Aiming at eliminating errors at yield strain, the strain in the range of 0.05-0.60 and corresponding stress were employed to calculate the coefficients in modified STG model (Ref 25). That is why this model shows a relatively low accuracy at the initial plastic deformation.

From Fig. 8 and 11, most of the data points predicted by the new constitutive model and the modified STG model lie fairly close to the experimental results, and the correlation coefficients, R , for two flow stress models are more than 0.95, indicating that a good correlation between the predicted and experimental data of two models was achieved. Given that correlation coefficient cannot fully express the accuracy of the predicted data, average absolute relative error ($AARE$,

expressed as Eq 16), root mean square error ($RMSE$, expressed as Eq 17) and maximum absolute error ($MAXE$, expressed as Eq 18) are applied as statistics estimators to evaluate the precisions of the models (Ref 27). In Eq 16-18, E_i is the experimental value, P_i is the predicted value, and N is the number of data points. To remove the influence of flow curves near the yield point, $AARE$ and $MAXE$ for modified STG model were calculated in the strain range of 0.05-0.60. Statistics estimators at each strain rate shown in Table 2 were the average values at different deformation temperatures but the same strain rate.

As shown in Table 2, the root mean square errors (RMSEs) for modified STG model are less than 13 MPa, and AAREs are

Table 2 Error evaluation criteria of calculated flow stress by the new constitutive model and modified STG model at different strain rate

Strain rate, s ⁻¹	New constitutive model			Modified STG model		
	AARE, %	MAXE, MPa	RMSE, MPa	AARE, %	MAXE, MPa	RMSE, MPa
0.1	2.65	7.90	3.74	3.41	9.16	4.30
1	1.50	8.51	2.97	4.05	14.17	7.68
3	2.15	17.26	5.86	6.39	19.80	12.06
10	2.25	9.94	5.53	2.07	11.33	4.96

also less than 7.00%. Regarding the new constitutive model proposed in the present paper, the values of RMSE and AARE are determined less than 10 MPa and 3.00%, respectively, indicating the new constitutive model can effectively predict flow behavior at different tempering temperatures and strain rates. Besides, it is clearly observed that the calculated values of the new constitutive model approximate well to the real ones, and are more accurate compared to those of modified STG model, which validates the new model is a reliable tool for predicting the changes in the flow stress of this material not only under state of equilibrium deformation, but also under condition of transient deformation. Besides, the new constitutive model was found still viable in the initial stage of plastic deformation where plastic strain is lower than 0.05.

$$\text{AARE}(\%) = \frac{1}{N} \sum_{i=1}^N \left| \frac{E_i - P_i}{E_i} \right| \times 100 \quad (\text{Eq 16})$$

$$\text{RMSE}(\text{MPa}) = \sqrt{\frac{\sum_{i=1}^N |E_i - P_i|^2}{N}} \quad (\text{Eq 17})$$

$$\text{MAXE}(\text{MPa}) = \text{Max}|E_i - P_i| \quad (\text{Eq 18})$$

4. Conclusions

In this paper, the thermal compressive deformation of hypereutectoid 95CrMo steel was carried out on a Gleeble-3500 thermo-simulation system over a practical range of deformation temperature (1073-1323 K) and strain rate (0.1-10 s⁻¹). The flow behavior under different deformation conditions was studied, and a constitutive model was developed. Conclusions are obtained as follows:

1. The true stress-strain curves of 95CrMo steel show that, with the increase in deformation temperature or decrease in strain rate, the peak strength during hot compressive process decreases. The dynamic recrystallization occurs when the strain rate is 0.1 s⁻¹ and temperature is more than 1173 K.
2. To model hot deformation behavior of 95CrMo steel, a new constitutive model was developed based on work-hardening law proposed by Sah et al. And the quantitative relationship of main parameters was determined and discussed. A comparison between the experimental and calculated values confirmed the reliability of this model. Correlation coefficient (*R*) and average absolute relative error (AARE) were found generally above 0.99 and be-

low 3.0%, respectively, which indicates a good predictability of the new constitutive model.

3. To further study the precision of the constitutive model proposed in the present paper, a relatively new model that was modified in Sellars-Tegart-Garofalo model (STG model) was introduced. Compared to the modified STG model, the new constitutive model exhibits a higher accuracy, which validates the new constitutive model is a reliable tool for predicting flow stress of this material not only under equilibrium deformation states, but also under transient deformation conditions. Besides, the new constitutive model was found still viable in the initial stage of plastic deformation where plastic strain is lower than 0.05.

Acknowledgments

The authors would like to acknowledge the found supported by the National Science & Technology Pillar Program during the Twelfth Five-year Plan Period (Grant Nos. 2012BAE03B01). The authors would like to thank Mr. Yan-Jun Yin and Mrs. Jin Guo for their great help in Gleeble experiments.

References

1. F. Yin, L. Hua, H.J. Mao, and X.H. Han, Constitutive Modeling for Flow Behavior of GCr15 Steel Under Hot Compression Experiments, *Mater. Des.*, 2013, **43**, p 393–401
2. T. Yan, E.L. Yu, and Y.Q. Zhao, Constitutive Modeling for Flow Stress of 55SiMnMo Bainite Steel at Hot Working Conditions, *Mater. Des.*, 2013, **50**, p 574–580
3. K.P. Rao, Y.K.D.V. Prasad, and E.B. Hawbolt, Hot Deformation Studies on a Low-Carbon Steel: Part 2—An Algorithm for the Flow Stress Determination under Varying Process Conditions, *J. Mater. Process. Technol.*, 1996, **56**, p 908–917
4. H.J. McQueen, S. Yue, N.D. Ryan, and E. Fry, Hot Working Characteristics of Steels in Austenitic State, *J. Mater. Process. Tech.*, 1995, **53**, p 293–310
5. M.P. Phaniraj and A.K. Lahiri, The Applicability of Neural Network Model to Predict Flow Stress for Carbon Steels, *J. Mater. Process. Technol.*, 2003, **141**, p 219–227
6. E.S. Puchi-Cabrera, J.D. Guérin, M. Dubar, M.H. Staia, J. Lesage, and D. Chicot, Constitutive Description of Fe–Mn23–C0.6 Steel Deformed Under Hot-Working Conditions, *Int. J. Mech. Sci.*, 2015, **99**, p 143–153
7. E.I. Galindo-Nava and P.E.J. Rivera-Díaz-del-Castillo, Thermostatistical Modelling of Hot Deformation in FCC Metals, *Int. J. Plast.*, 2013, **47**, p 202–221
8. J.P. Sah, G. Richardson, and C.M. Sellars, Recrystallization During Hot Deformation of Nickel, *J. Aust. Inst. Met.*, 1969, **14**, p 292–297

9. Y.C. Lin, M.S. Chen, and J. Zhong, Prediction of 42CrMo Steel Flow Stress at High Temperature and Strain Rate, *Mech. Res. Commun.*, 2008, **35**, p 142–150
10. F.A. Slooff, J. Zhou, J. Duszczek, and L. Katgerman, Constitutive Analysis of Wrought Magnesium Alloy Mg–Al4–Zn1, *Scripta Mater.*, 2007, **57**, p 759–762
11. Y.C. Lin, M.S. Chen, and J. Zhong, Constitutive Modeling for Elevated Temperature Flow Behavior of 42CrMo Steel, *Comput. Mater. Sci.*, 2008, **42**, p 470–477
12. W. Yu, L.X. Xu, Y. Zhang, and E.T. Dong, Constitutive Equation for High Temperature Flow Stress of 95CrMo Steel, *Trans. Mater. Heat Treat.*, 2016, **10**, p 261–267
13. E.S. Puchi-Cabrera, M.H. Staia, J.D. Guérin, J. Lesage, M. Dubar, and D. Chicot, Analysis of the Work-hardening Behavior of C-Mn Steels Deformed Under Hot-Working Conditions, *Int. J. Plast.*, 2013, **51**, p 145–160
14. D.L. Hong, T.H. Gu, and S.G. Xu, *Drill Tool and Drill Steel*, Metal Industry Press, Beijing, 2000, p 121–134
15. Z.S. Wang, W. Yu, J.Z. Xiong, W.L. Tang, J.J. Yu, and J.Z. Zhang, Researches on Dynamic and Static Transformations of 95CrMo Drill Steel, *J. Iron Steel Res.*, 2009, **159**, p 22–25
16. N.Q. Peng, G.B. Tang, J. Yao, and Z.D. Liu, Hot Deformation Behavior of GCr15 Steel, *J. Iron. Steel Res. Int.*, 2013, **20**, p 50–56
17. J.G. Zhang, D.S. Sun, H.S. Shi, and H.B. Xu, Microstructure and Continuous Cooling Transformation Thermograms of Spray Formed GCr15 Steel, *Mater. Sci. Eng., A*, 2002, **326**, p 20–25
18. H. Chen, Heat Treatment Process of the 95CrMo Conical Drill Rod, *Mod. Mach.*, 2014, **01**, p 75–78
19. Y.Q. Song, Z.P. Guan, P.K. Ma, and J.W. Song, Theoretical and Experimental Standardization of Strain Hardening Index in Tensile Deformation, *Acta Mater. Sinica*, 2006, **42**, p 673–680
20. D. Samantaray, S. Mandal, C. Phaniraj, and A.K. Bhaduri, Flow Behavior and Microstructural Evolution During Hot Deformation of AISI, Type 316 L(N) Austenitic Stainless Steel, *Mater. Des.*, 2011, **32**, p 2797–2802
21. C. Zener and J.H. Hollomon, Problems in Non-Elastic Deformation of Metals, *J. Appl. Phys.*, 1944, **15**, p 22–27
22. S.A. Krishnan, C. Phaniraj, C. Ravishankar, A.K. Bhaduri, and P.V. Sivaprasad, Prediction of High Temperature Flow Stress in 9Cr–1Mo Ferritic Steel during Hot Compression, *Int. J. Pres. Ves. Pip.*, 2011, **88**, p 501–506
23. D.W. Suh, J.Y. Cho, O.K. Hwan, and H.C. Lee, Evaluation of Dislocation Density from the Flow Curves of Hot Deformed Austenite, *ISIJ Int.*, 2002, **42**, p 564–566
24. A. Yoshie, T. Fujita, M. Fujioka, K. Okamoto, and H. Morikawa, Formulation of Flow Stress of Nb Added Steels by Considering Work-hardening and Dynamic Recovery, *ISIJ Int.*, 1996, **36**, p 467–473
25. F. Yin, L. Hua, H.J. Mao, X.H. Han, D.S. Qian, and R. Zhang, Microstructural Modeling and Simulation for GCr15 Steel during Elevated Temperature Deformation, *Mater. Des.*, 2014, **55**, p 560–573
26. C.X. Yue, L.W. Zhang, S.L. Liao, J.B. Pei, H.J. Gao, Y.W. Jia, and X.J. Lian, Research on the Dynamic Recrystallization Behavior of GCr15 Steel, *Mater. Sci. Eng., A*, 2014, **339**, p 560–573
27. B.S. Xie, Q.W. Cai, W. Yu, J.M. Cao, and Y.F. Yang, Effect of Tempering Temperature on Resistance to Deformation Behavior for Low Carbon Bainitic YP960 Steels, *Mater. Sci. Eng., A*, 2014, **618**, p 586–595